First Light Adaptive Optics System for Large Binocular Telescope

S. Esposito[a], A. Tozzi[a], D. Ferruzzi[a], M. Carbillet[a], A. Riccardi[a], L. Fini[a], C. Verinaud[a], M. Accardo[a], G. Brusa[a], D. Gallieni[b], R. Biasi[c], C. Baffa[a], V.Biliotti[a], I. Foppiani[d], A. Puglisi[a], R. Ragazzoni[a], P. Ranfagni[a], P. Stefanini[a], P. Salinari[a], W. Seifert[e], J.Storm[f]

[a] Osservatorio Astrofisico di Arcetri, Largo E. Fermi 5, 50125 Firenze, Italy
[b] ADS International, Corso Promessi Sposi 23/d, 23900 Lecco Italy
[c] Microgate Srl, Via Kravogl 8, 39100 Bolzano, Italy
[d] Dipartimento di Astronomia, Universita di Bologna, Via Ranzani 1, 40127 Bologna, Italy
[e] Landessternwarte, Königstuhl 12 D-69117 Heidelberg, Germany
[f] Astrophysikalisches Institut Potsdam, An der Sternwarte 16, D - 14482 Potsdam, Germany

ABSTRACT

The paper describes the design of the single conjugate Adaptive Optics system to be installed on the LBT telescope. This system will be located in the Acquisition, Guiding and Wavefront sensor unit (AGW) mounted at the front bent Gregorian focus of LBT. Two innovative key features of this system are the Adaptive Secondary Mirror and the Pyramid Wavefront Sensor. The secondary provides 672 actuators wavefront correction available at the various foci of LBT. Due to the adaptive secondary mirror there is no need to optically conjugate the pupil on the deformable mirror. This allows having a very short sensor optical path made up using small dimension refractive optics. The overall AO system has a transmission of 70 % and fits in a rectangle of about 400x320mm. The pyramid sensor allows having different pupil sampling using on-chip binning of the detector. Main pupil samplings for the LBT system are 30x30, 20x20 and 10x10. Reference star acquisition is obtained moving the wavefront sensor unit in a field of view of 3x2 arcmin. Computer simulations of the overall system performance show the good correction achievable in J, H, and K. In particular, in our configuration, the limiting magnitude of pyramid sensor results more than one magnitude fainter with respect to Shack- Hartmann sensor. This feature directly translates in an increased sky coverage that is about doubled with respect to the same AO system using a Shack-Hartmann sensor.

Keywords: Pyramid Wavefront Sensor, Achromatic Pyramid, First Light LBT

1. INTRODUCTION

First light of LBT telescope[1] is foreseen in summer 2004 and adaptive optics is supposed to start from the beginning. The Adaptive Optics system to be used in first light is part of the Acquisition, Guiding and Wavefront sensing unit[2] (AGW) mounted inside the instrument derotator of the front bent Gregorian foci of the telescope. This unit is providing telescope guiding, active and adaptive optics correction and contains all the AO system opto-mechanics and electronics. The only exception to this is the system Deformable Mirror (DM) that in the LBT case is the telescope adaptive secondary mirror[3]. The instrument coupled with the AO system is the LBT common user instrument called LUCIFER[4]. This instrument is mounted on the same instrument derotator of the AGW unit. Diffraction limited operating modes of LUCIFER are NIR imaging with a 30”x30” FOV and

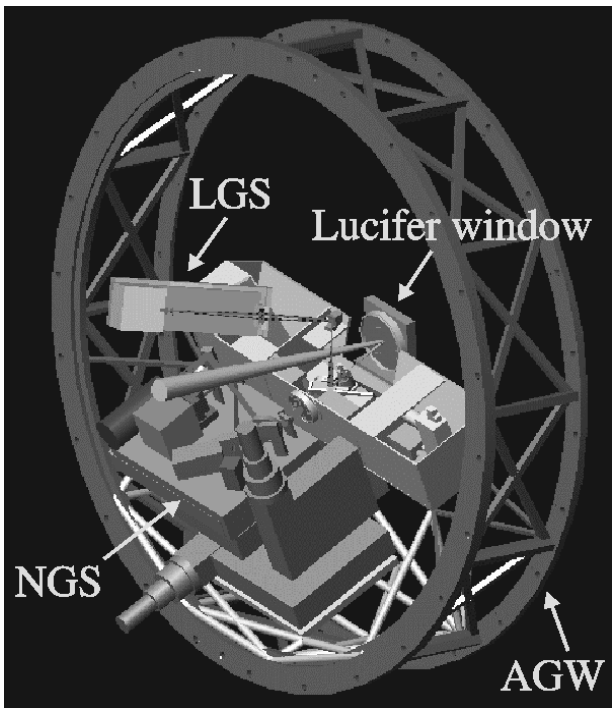

Fig 1. Natural Guide Star (NGS) and Laser Guide Star (LGS) WFSs arranged inside the AGW structure. The blue beam represents light coming from the telescope

long slit spectroscopy with spectral resolution in the range 21000-37000. The instrument wavelength range is 0.9-2.5 μm. The AO system will have in first light a Natural Guide Star WFS. However a Sodium Laser Guide Star (LGS) WFS has been designed and can be realized and installed in the future. During operation with the LGS WFS the NGS WFS unit will provide the tip-tilt signal. Both NGS and LGS WFSs are Pyramid wavefront sensors. Pyramid wavefront sensor[5] has been chosen because of the better performance achievable with respect to Shack-Hartmann sensor when a NGS is used and, in general, because it is easily reconfigurable in terms of pupil sampling and sensor sensitivity[6,7] as described later. The arrangement of the two WFSs inside the AGW structure is reported in **fig. 1**. Finally a NIR tip-tilt sensor is available and is located inside LUCIFER. This sensor allows correcting for atmospheric image motion and differential flexure between the AO system and LUCIFER. The paper describes the various parts of the AO system except for the adaptive secondary unit named LBT672 that is described in a different paper of this proceeding[3].

2. NATURAL GUIDE STAR WAVEFRONT SENSOR BOARD

The NGS wavefront sensing unit is realized using very small and standard optical elements. This is possible for two reasons: the first one is the use of the adaptive secondary mirror[3,8] so that we have not to conjugate the telescope pupil to the DM in the optical train of the WFS, the second is the adoption of a moveable WFS unit to achieve the requested Field-Of-View (FOV) of 2 arcminute diameter, easy upgradeable, to 3x2 arcmin, for reference star acquisition. Using this approach, we have designed a WSF board of dimension 320x400mm. The board hosts two sensing channels: one for the pyramid wavefront sensor, the other providing an f/45 focal plane for AO system testing and source acquisition. The WFS optical train total length is about 500mm. The diameter of the refocusing and camera lens used are 32 and 10 mm respectively. A fixed WFS solution of the same total length having a FOV of 2 arcmin diameter requires an f/1.6 field re-imaging optics of diameter 80 mm. Analysis of the fixed WFS optical design has shown that the reimaging optics is quite critical in terms of misalignment of the various components, so that we preferred a moveable WFS solution. The compact WFS board has several important features, with respect to a fixed WFS with parts directly mounted on the AGW structure. Main advantages are: reduced size and cost of the optical elements, low number of optical surfaces giving high efficiency of the optical train, the short system length reduces system internal flexure and turbulence effects along the optical path, very low non common path aberration vs. FOV, easy assembly and testing of the unit as a stand alone unit.

2.1 WAVEFRONT SENSOR OPTICAL DESIGN

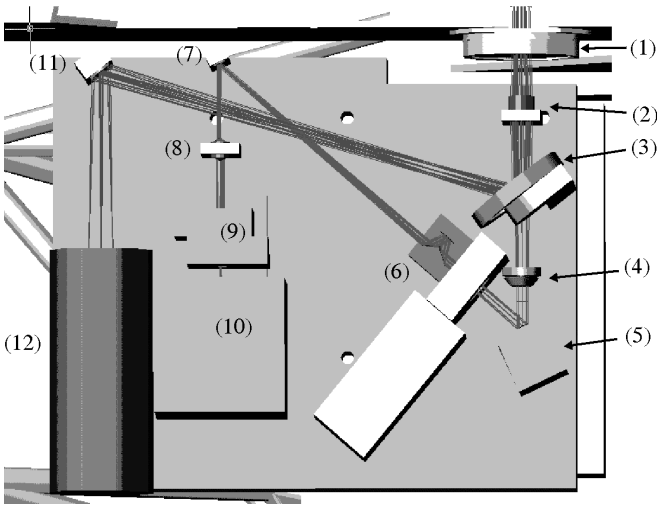

Fig 2. The NGS wavefront sensor board. The filter wheel (3) controls the light shearing between the pyramid WFS (transmitted light) and the technical viewer (reflected light)

An AUTOCAD drawing of the NGS board including the ZEMAX drawings of the two channels, one for the WFS optimized in the wavelength range 0.6 – 0.9 μm, and one for the acquisition camera, is reported in **fig. 2**. The light analyzed by the wavefront sensor is reflected off by the LUCIFER entrance window that is tilted to 15° with respect to the incoming beam of the telescope. In the present design the board is moveable in X and Y of 108x72 mm. This allows obtaining an acquisition FOV of 3x2 arcmin. The first optical element in the WFS optical path is the telecentric lens (1) that in this drawing has a diameter of 80mm. Thirty millimeters after this lens we found a refocusing triplet (2) that provides an f/45 beam on the top of the pyramid. After the triplet we found a filter wheel (3) that controls the light shearing between the pyramid WFS and the acquisition camera. Light for the acquisition camera (12) is reflected by a 50/50 beam splitter for technical use or by a dichroic filter reflecting

the short wavelengths during reference acquisition. Finally during AO observation a third position of the wheel allowed to transmit all the light to the WFS. Light transmitted to the WFS is passing through an Atmospheric Dispersion Corrector (ADC) (4) before reaching a commercial piezo-driven fast steering mirror (5). The refocusing triplet is creating an image of the telescope pupil (the adaptive secondary) on the steering mirror. This mirror provides the tilt modulation needed to operate the pyramid sensor. The tilt modulation range of the mirror is +/- 0.8 arcsec. The pyramid vertex is placed in the f/45 focal plane and 44 mm after the pyramid a camera triplet (9) of 35 mm focal length and 10 mm diameter is creating four pupil images onto the CCD sensor (10). During observations the actuator positions in the pupil images are changing with time being the board placed inside the instrument derotator. To avoid this we introduced a three mirrors pupil re-rotator (6) between the steering mirror and the focal plane. In this configuration we have four motorized rotation axes to control the optical elements (3,4,6). A critical issue in the pyramid sensor optical set-up is the camera triplet displacement that changes the pupil positions on the CCD as is showed in section 5. To ensure proper positioning of this element we are considering two options: to co-mount the lens with the CCD head or to have three translation stages with sub μm accuracy to compensate for lens misalignment. This compensation can be done measuring the actual pupils position with the sensor.

2.2 THE PYRAMID

The fundamental optical component of the WFS is the refractive pyramid. This part is designed so to have an angularly well-packed set of four pupils coming out from the pyramid. The minimum angular separation to avoid pupil superposition when opposite to vertex beams are considered is $\sqrt{2}/f_n$ where f_n is the f-number of the beam reaching the pyramid. In this condition the pupil centers are arranged in a square grid of angular side $1/f_n$. The base angle of a single pyramid that introduces this separation, in our case where f_n=45, is readily founded to be about 2^o. The pyramid designed for the WFS is made of two square base pyramids attached for the base[10]. This double pyramid introduces an angular separation between the two opposite outcoming beams given by $\delta = \alpha_1 (n_1 - 1) - \alpha_2 (n_2 - 1)$ where δ is half of the requested angular separation; α_1, α_2 are the two base angles for the two pyramids and n_1, n_2 are the refractive indexes of the two glasses. So the considered pyramid is acting as a single pyramid having an effective base angle equal to the difference of the base angles of its two components. This allows working with quite large base angles like 30^o that greatly simplify the optical polishing of the pyramid edges. Scratched edges of the order of 10 μm (overall scratched width is 20 μm) would be a problem for the AO system when in closed loop operation the sensor PSF at 0.75 μm approaches the diffraction limited FWHM of

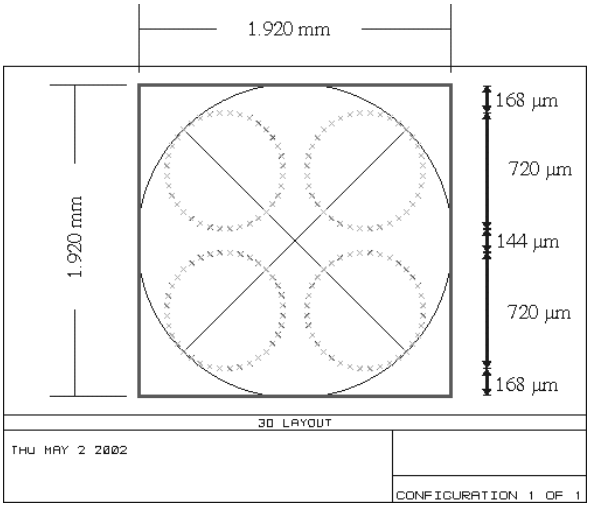

Fig 3. Pupils arrangement on the CCD surface: the square is the surface of Marconi EEV39 CCD.

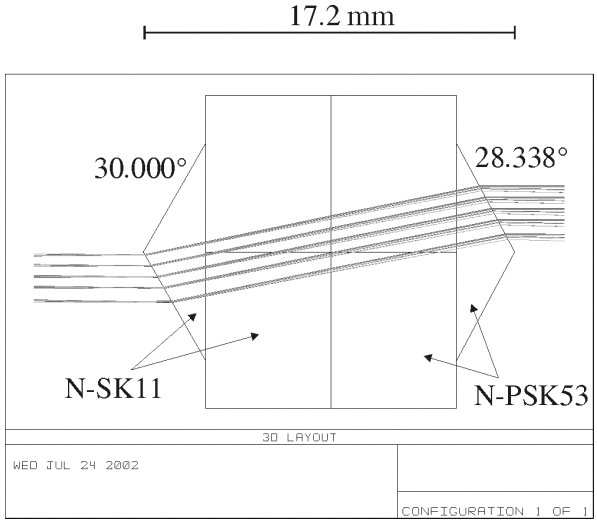

Fig 4. The optical design oh the pyramid after the optimization with ZEMAX. The represented five fields are 0.07", 0.34", 0.62", 0.9", 1.24". Light propagation left to right.

33.7 μm. The loss of energy due to the edges in this case is 54%. We estimate that the polishing of two pyramids both with base angles of about 30° should lead to scratched edges less than 2 μm leading to an energy loss lower than 10%. The overall transmission of the WFS channel considering the pyramid losses is 72%. To correct for chromatic aberrations we need to use two different glasses. The obtained pyramid optical design after optimization with ZEMAX is showed in **fig. 4** together with the pyramid principal characteristic. The pyramid FOV for this design is 2.5 arcsec. In our set-up the camera triplet focal length has been chosen in order to have 30 pixels of the WFS detector (24 μm pixel size) on a pupil diameter and six pixels between the edges of two different pupils. Moreover the angular separation is calculated so that the centers of the pupil fall in the middle of a CCD pixel. The arrangement of the pupils on the WFS CCD chip, (the Marconi EEV39) is reported in **fig. 3**. Residual aberration and chromatism of the WFS channel lead to a pupil images distorsion of about 1 μm rms inside a 1 arcsec FOV. We require the pupil positioning error due to polishing accuracy to be less than 1/10 of the CCD pixel size. This leads to a pyramid base angle error less of 10 arcsec and a pyramid thickness error less than 50 μm.

2.3 WAVEFRONT SENSOR DETECTOR

The baseline for the high order channel detector is a camera system based on the 80x80 pixel Marconi chip CCD39 produced by SciMeasure inc. Atlanta (USA). The CCD39 chip has a pixel size of 24x24μm and an overall dimension of 2x2mm. To match the quantum efficiency of the chip with the spectral region where wavefront sensing is taking place (0.6-0.9 μm) we selected a deep depletion silicon chip. The QE of this device together with the standard one is reported in **fig. 5**. Average QE in the WFS band is 81% and 59% for deep depletion and standard chip respectively. The camera system can run at different frame rates using four basics pixel rates. The control electronics has four analog filters that are optimized to minimize Read Out Noise (RON) at those pixel rates. Optimal pixel rates for LBT system are 150, 400, 850 and 2500 KHz. Basics CCD driving waveforms allow running the system at 100, 200, 400, 600 and 1000 frame/s. Other driving waveforms are provided to achieve x2, x3 and x5 on-chip binning. Moreover modifications of these sequences are available to reduce the dark current value using dithering operation. The obtained RON values are between 3.5 and 8.5 e^- depending on the considered pixel rate and binning. Other noise sources are the dark current and the sky background. The last ones results negligible in the sensing band contributing less than 1e^- even in case of long integration time 10ms and high binning 5x5. Dark current can give a significant contribution in the considered condition being bigger than read out noise. Pixel noise as a function of integration time, pixel rate and binning are reported in **fig. 6**. Discontinuities in the reported curves are due to change of the pixel read out speed accordingly to the requested integration time. Calculations for dark current are carried

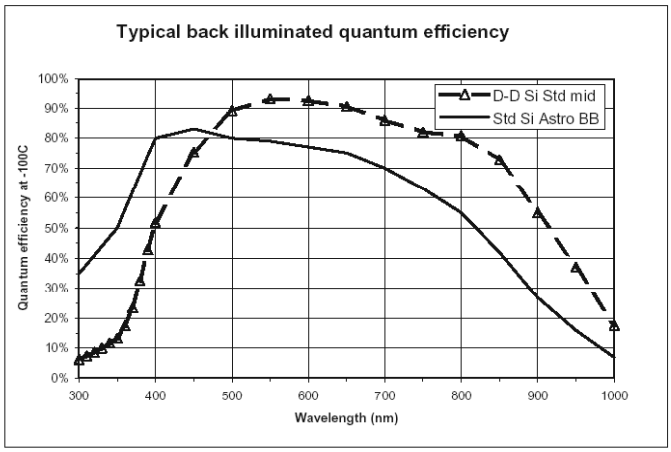

Fig 5. QE of the Marconi chip CCD39 for standard chip (continuos) and deep depletion chip (triangles).

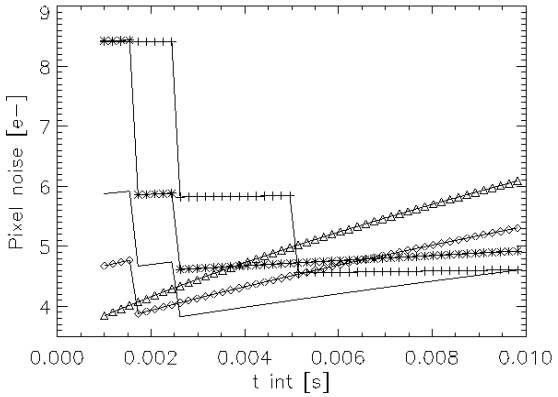

Fig 6. Pixel noise as a function of integration time and for x1 (cross), x2 (asterisk), x3 (line) ,x4 (diamond) and x5 (triangle) binning modes are reported.

out supposing a chip temperature of –40°C and a dark current rate of 10^2 e^-/pixel/second (nominal EEV performance). However the dark current rate is strongly dependant on the chip temperature so that at –30°C it becomes five times bigger. So we are considering the option to use another cooling stage in addition to the Peltier cooling to get lower temperatures of the chip. The development of a camera system based on the new Marconi chip LLL CCD60 is an ongoing joint program between the Arcetri and Bologna Observatory[15]. This chip has a read out noise lower than $1e^-$ even at a frame rate of 1000 frame/s. Because the pixel dimension of this chip is the same of the CCD39 we can easily upgrade the wavefront sensor camera when the new camera system will be available.

3. WFS BOARD POSITIONING

The NGS WFS is translated in the telecentric field to acquire the reference source. This means to get the proper focus and the proper centering of the reference star on the pyramid. This is achieved using the three translation stages that define the board position. The arrangement of the considered stages with respect to the board is reported in **fig. 7**. The stages that we selected for the system are commercial stages produced by Bayside Motion Corporation. Nominal pitch and yaw of the stages are less than 2.5 arcsec and fulfill the opto-mechanical tolerances for the WFS optical path. Accuracy and repeatability of the stages positioning are less than 2.5 μm. The main limitation in term of system absolute positioning and stability comes from the flexures of the translation stages, of the stages supporting structure, and of the AGW structure itself. Finite Elements analysis of the WFS board displacements and tilt was performed by ADS. The analysis considered 24 load cases. The first 12 took into account three zenith distances for telescope pointing z = 0°, 25°, 50° and four derotator positions 0°, 90°, 180°, 270°. Other 12 cases took into account the same zenith distances and four different derotator positions 15°, 105°, 195°, 285°. The stage stiffness was assumed equal to 50N/μm. The displacements and tilts of the board with respect to the nominal position in these 24 load cases were in the range of +/-96 μm and +/-42 arcsec respectively. Both errors lead to a PSF displacement in the f/45 wavefront sensor focal plane. The PSF angular displacement with respect to nominal position due to these flexures is 0.17 and 0.1 arcsec for board displacement and tilt respectively. These numbers shows that system flexures do not locate the reference star outside the sensor FOV of 2.5 arcsec diameter. Moreover accurate centering of the star on the pyramid vertex can be done simply closing the adaptive loop. The required PSF displacement (0.2 arcsec) can be easily introduced using the adaptive secondary or the fast steering mirror. This last option will however reduce the available modulation range of about 10 %. To study the system stability during observations we evaluated the rates for displacements and tilt of the WFS board for small rotation of the derotator. These rates were obtained using the 12 couples of load cases with the derotator position increased by 15°. All of the displacements and tilts rate that we found were lower than 1.46 μm/° and 0.58 arcsec/° respectively. Only in the case of z = 50° and derotator position 180° we found 6.6 μm/° and 1.96 arcsec/°. Supposing a derotation speed of 15 °/h we have a PSF displacement of 1.9 μm in five minutes due to board displacement and tilt. The overall displacement obtained in this case is about 1/10 of LUCIFER diffraction limited PSF at 1.25 μm. The LUCIFER infrared tip-tilt sensor, having a FOV of about 2 arcmin diameter, can be used to correct for this effect of differential flexures. This sensor is providing the AO system with a long integration signal to compensate for flexures. Numbers reported above showed that a tip-tilt sampling at about one-minute rate is adequate to correct for flexures. LBT telescope receives in an integration time of 60 seconds about 10^4 photons from a star of H mag 20. So sky coverage for differential flexure is not a problem. The tilt correction can be done using the steering mirror and off loading accumulated errors to the stages. It is interesting to note that the stages

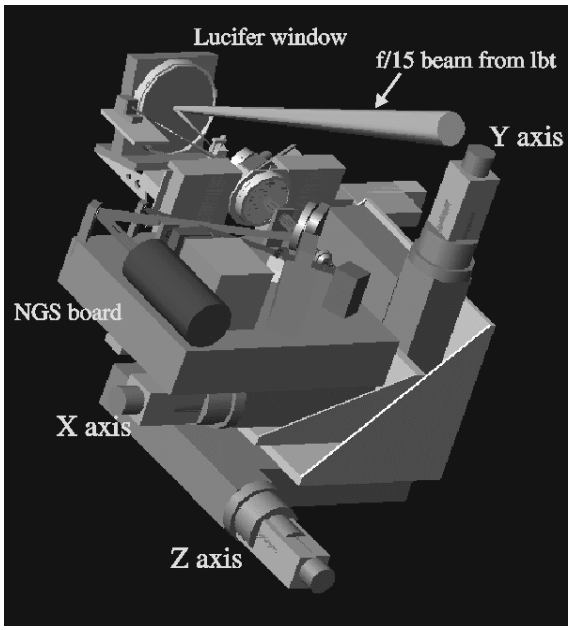

Fig 7. The arrangement of the XYZ stages, produced by Bayside Inc., with respect to the WFS board and telescope incoming beam.

can be used to track non-stellar reference object like asteroids planets and so on. To monitor the system during daylight test and to simplify the star acquisition operation the WFS board host a second optical channel that is providing an f/45 focal plane. The FOV available for star acquisition is limited by the detector size. The considered detectors for this channel are the Marconi LLL CCD65 that has a sensitive area of 11.5x8.6 mm leading to a FOV of 6.4x4.8 arcsec or a standard intensified CCD with a larger FOV of about 10 arcsec.

4. SODIUM LASER GUIDE STAR WAVEFRONT SENSOR

The LBT first light AO system is designed to have a laser guide star wavefront sensor in addition to the NGS WFS. This is a pyramid wavefront sensor quite similar to the NGS WFS. However the use of the laser guide star that is seen from the telescope as an extended object of 1 – 2 arcsec diameter simplify the optical design of the sensor. First the wavefront modulation is not required so we do not need to insert the steering mirror in the optical design, second the pyramid edges are no longer a critical issue because the PSF dimension even in the f_{15} focal plane is ranging between 0.6 and 1.2 mm. Edges of 10 μm, achieved with polishing of single pyramid (4) with small base angles, are fully acceptable. The LGS WFS unit is moveable along the optical axis to re-focus the system on the sodium layer when the telescope is pointing in the range 0^o – 70^o of Zenith. The sodium light is reflected by a tilted dichroic (1) located close to the LBT reflected focal plane. The transmitted light is used in the NGS WFS to measure the tilt signal not available from the LGS. The optical design of the LGS unit is a simplified version of the NGS WFS. Main optical elements are a refocusing lens (3) and a camera lens (5). In this case the refocusing lens is not changing the beam f/ but is used to get some space in order to focus the system on the sodium layer for different telescope pointing positions. **Fig. 8** reports the LGS WFS optical design. The picture reports two configurations of the unit one for zenith pointing and one for 70 deg pointing. The travel range requested to achieve both positions is 110mm. The camera lens is such that the pupil arrangement in the image plane is the same of the NGS WFS. We are planning to use as WFS camera the same camera system that is the baseline system for the NGS WFS. Changing the basic pupil sampling accordingly to the laser returned number of photons is easy changing the focal length of the camera lens. Finally we note that the translation stages selected for the LGS WFS unit produced by Physic Instrumente, (Germany) has a maximum speed of 3mm/s. This means that we can track the temporal variation of the baricenter of the sodium spot slower than 1.5 km/s.

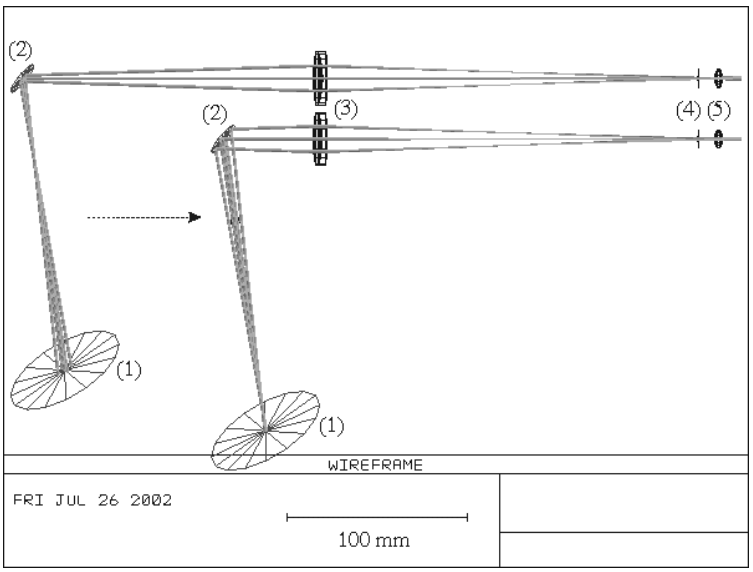

Fig 8. Two configurations of the LGS WFS unit: one for zenith pointing (right) and one for 70 deg pointing (left). The travel range is 110 mm. Displacement of the pyramid optical axis is introduced for clarity.

5. AO SYSTEM ARCHITECTURE AND REAL TIME OPERATION

The AO system block diagram is reported in **fig. 9** and is made up of four main blocks plus the user interface. The AO supervisor is a standard PC running RT-Linux and has complete control of the AO system. It controls the system operating modes, sends parameters and commands to the different subsystems and gathers telemetry and diagnostic data. It also communicates with the Telescope Control System (TCS) for coordination with the other telescope subsystem. All the subsystems listed in **fig. 9** are provided with an Ethernet channel by which control and diagnostic

data can be exchanged with the supervisor. The supervisor software will have essentially two operating modes: a standalone mode to allow tests and engineering activities and an observation mode in which it behaves as a slave to receive commands from the TCS. The fast real time data flow for AO operation is going through a different fiber link with a dedicated protocol that connects the WFS detector, the slope computer, and the control electronics of the adaptive secondary, the last providing slopes to wavefront calculations and actuators control. The wavefront reconstruction process and the dedicated hardware in the LBT system is divided in two parts physically placed at two different locations. The slope computer[11] is a custom board that has been developed by MicroGate (Italia) mainly as a communication control board for the adaptive secondary. This board is placed close to the WFS detector inside the AGW unit. The fast matrix multiplier is obtained using the 336 DSPs located aboard the LBT672 adaptive secondary[11]. These DSPs are normally used to control the position loop of the adaptive secondary actuators. In particular each DSP is providing control for two actuators. This network of DSPs can be used to parallelize the matrix multiplication. This is very important for LBT first light AO system where the reconstruction matrix can be as big as 1400x672 requiring a single DSP capable of tens of Gflop/s to perform the requested multiplication. The pixel acquisition is obtained, when using the EEV39 chip based camera, through 72 reconfigurable digital IO lines (PIO) placed on the slope computer board. This board uses a DSP having a speed of 380 MAC/s to calculate the wavefront slopes. Pixel values are transferred to the DSP using a DMA channel and the 64 bit DSP bus running at 2.9 Gbit/s. The slopes are sent to the adaptive secondary mirror using a high-speed fiber link (2Gb/s). A board similar to the slope computer board but placed at the secondary mirror receives and dispatches the slopes to all the 336 DSPs. Each of the DSPs has two lines of the reconstructor matrix stored in memory and perform the scalar product between the signals and the matrix coefficients finding the commands for a couple of actuator. The reconstruction process described above for a zonal reconstructor can be easily extended to a modal reconstructor where all the modes have the same time filtering function. Different time filtering of the various modes requires to know and to save the modal coefficients at the various iterations. This feature is implemented in the wavefront reconstructor. In the case of EEV39 chip when no binning is applied, the time delay between start of CCD frame readout and end of mirror command computation is as following: readout time 920 μs, slope computing time starting at half of frame readout time 120 μs, slope transfer to wavefront reconstructor 27 μs, mirror command calculation 41 or 57 μs for zonal or modal control respectively. This gives a total delay time of 1 ms dominated by CCD readout time. In the case of the LLL CCD the readout time is 256 μs. All the others delay times remain unchanged so that the overall delay time is reduced to 336 μs. Connection of the CCD control electronics to the slope computer is in this case obtained through a the fast fiber link.

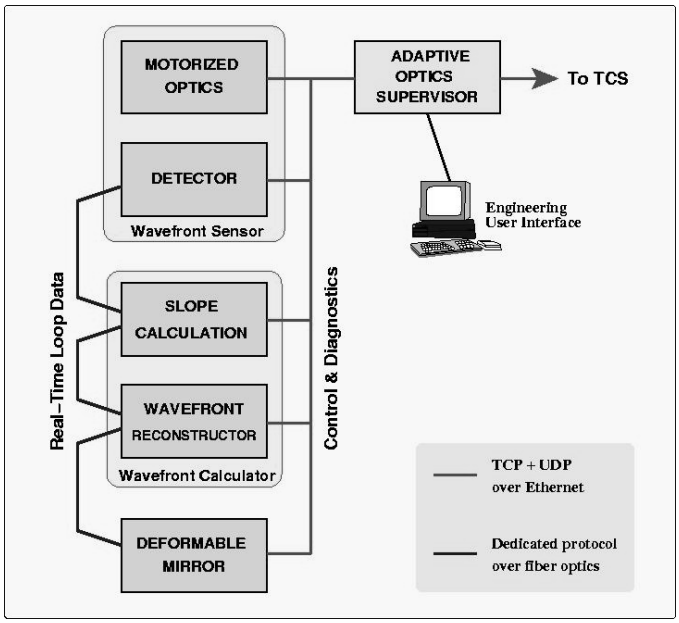

Fig 9. The block-diagram of the adaptive optics system. The left link is the fast link used for the real time AO control loop.

6. OPTO MECHANICAL TOLERANCES

We have calculated the opto mechanical tolerances with respect to misalignments (*dx, dy, dz*) and tilt (*tx, ty*) of the main opto mechanical parts encountered in the WFS optical path. This analysis is aimed to investigate the pupil image quality on the WFS CCD: to do this we define a Merit Function (MF) measuring the pupil image aberrations calculating the rms of the ray actual positions with respect the nominal one in different points in pupil image, for different wavelengths and fields. We report the results as rate of variation of the MF with respect to the changing parameter (CP): for *(dx, dy, dz)* the results are given as μm/μm, for *(tx, ty)* as μm/arcsec (i.e. variation of MF / variation of CP). The results are listed in **Table 1**. This table shows that the most critical issue for pupil positioning is the displacement of the camera

triplet having a displacement rate of 1.0. We are currently testing different kind of translation stages to evaluate if we can actively control the positions of this optical element. This is done in order to adjust the pupil position during the AO observation. Another option is to mount the camera lens directly on the CCD camera. Using the calculated rates we can estimate an overall error due to tilt and displacement of the optical elements mounted on the board except the camera triplet. To calculate the overall error we assume for the different optical parts 20μm and 10 arcsec of displacement and tilt error respectively. The overall error assuming uncorrelated misalignment results 2.7 μm and is mainly due to the tilts of the folding mirror. This error can be reduced to less than 2 μm assuming a tilt of 5 arcsec for the folding mirror. For the pupil re rotator, a critical moveable element, we have selected a commercial rotation stage (Micos Gmbh) that

	Lucifer window	**Telecentric lens**	**WFS board**	**refocusing triplet**	**Pupil rerotator**	**Fold mirror**	**Pyramid**	**Camera triplet**
dz	$8.6*10^{-4}$	$4.5*10^{-6}$	$2.4*10^{-5}$	$3.7*10^{-2}$	$1.2*10^{-3}$	$2.5*10^{-2}$	$4.5*10^{-4}$	1.0
dx, dy	0 , $7.4*10^{-4}$	$3.0*10^{-4}$	$9.0*10^{-4}$	$4.1*10^{-2}$	$4.5*10^{-2}$	$1.6*10^{-2}$	$1.6*10^{-4}$	1.0
tx	$4.3*10^{-2}$	< 0.01μm/º	$2.6*10^{-2}$	$2.4*10^{-3}$	$4.2*10^{-2}$	$1.4*10^{-1}$	$2.1*10^{-4}$	$5.0*10^{-3}$
ty	$4.6*10^{-2}$	< 0.01μm/º	$2.4*10^{-2}$	$2.6*10^{-3}$	$4.2*10^{-2}$	$1.6*10^{-1}$	$1.4*10^{-4}$	$5.9*10^{-3}$

Table 1. The opto mechanical tolerances calculated using Zemax for pupil image quality of the WFS. Numbers represents rates giving the ray rms in the pupil image as μm/μm or μm/arcsec

features a wobble and eccentricity error less than 4 arcsec and 6 μm respectively, so having misalignment errors better than those assumed in the error budget calculations. Another part of the error budget for pupil position is due to WFS board and LUCIFER window misalignments. We assume for the board misalignments the values found with FEA in section 3. In particular we take for the board displacements a value of 96 μm and for the tilt a value of 32 arcsec that is a limiting value bigger then the 88% of the determined board tilts. For the LUCIFER window we assume as a conservative estimate the same values for misalignments of those we have found for the WFS board. Using rates reported in **Table 1** and considering on-board error, WFS board and LUCIFER window misalignments we found an overall error of 3 μm, so about 1/8 of the CCD pixel size.

7. AO SYSTEM PERFORMANCE SIMULATIONS

We report in the following the results of computer simulations aiming to quantify the system performance in terms of achieved Strehl ratio in the J, H, and K band. The principal parameters of the simulations[12,13] are reported in **Table 2**.

Parameter	Simulation values
Atmospheric parameters	Two layers with wind velocity 15 m/s Fried parameter 15cm @500nm => 0.67 arcsec Turbulence outer scale 40m
Guide Star	Spectral type K5 V-magnitude in range 9.85—17.5
Telescope	Diameter 8.25m Obstruction ratio 0.11
Pyramid Wavferont Sensor	WF sampling: 10x10, 15x15, 30x30 (obtained using on chip binning) Exposure time: in range 1 – 10ms RON from 3.5 to 8.4 e- according to frame rate (SciMeasure camera specs) Tilt modulation: ±1 ±2 (30x30sub), ±3 (15x15sub), ±4,±5,±6 (10x10sub) λ/D
Transmission	0.9^3 * 0.7 * CCD QE = 0.4 (CCD average QE = 0.8 @ [600—900 nm]
Wavefront reconstructor	Reconstructed LBT672 mirror modes: 36,44, 55 and 66 => 10x10 conf. 78, 105 and 136 => 15x15 conf. 231, 351 and 496 => 30x30 conf
Time Filtering	Pure integrator with gain = 0.5

Table 2. Principal parameters used in the simulations[12,13]

For comparison purpose we calculated the SR using a Pyramid Sensor or using a Shack-Hartmann sensor with the same number of subapertures.

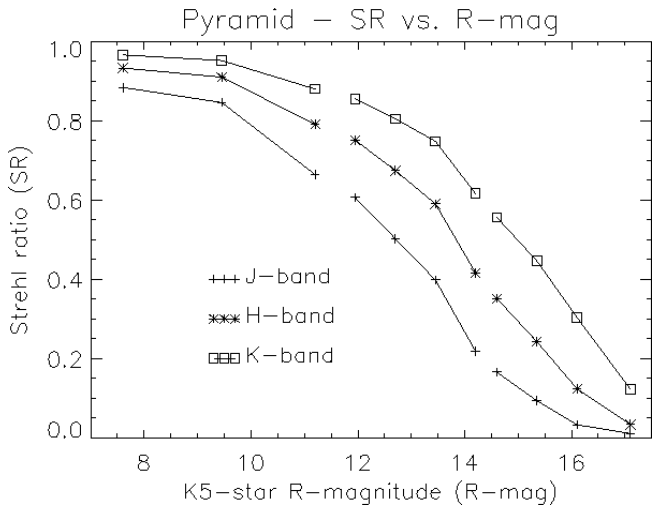

Fig 10. SR obtained as a function of the reference star magnitude for J,H,K bands

We calculate the best SR achievable as a function of the reference star magnitude using the various configurations for the WFS outlined in **table 2**. The optimized parameters are the number of sensing subapertures, the number of corrected modes, the value of the tilt modulation and the integration time. Results for J,H, and K bands for Pyramid Sensor (PS) are plotted in **fig. 10**. The first three curves on the left refer to 30x30 configuration and J, H and K SRs. The second group is obtained using 15x15 configuration and the last group is obtained using 10x10 configuration. The plot in **fig. 11** compares the results of PS with SHS in K band showing the pyramid gain located especially around magnitudes 15-16. In this range the PS obtain the same SR of the SHS using a star about one magnitude dimmer. This difference in limiting magnitude has the effect of increasing the system sky coverage with respect to the SHS. By using the Bahcall and Soneira model of star distribution[14] we can estimate the number of stars per square degree having magnitude less than a certain value. To estimate the system sky coverage, when a certain on axis Strehl ratio is desired, we have to take into account the maximum correction angle considered. Let's note it θ_{max} and take for it 30 arcsec in K-band. The corresponding area of sky is then $\pi\,\theta^2_{max}$, and the sky coverage is then 1-exp(-N) where N is the number of stars of a given R-magnitude in that area. Let's also consider a minimum Strehl ratio of 20% that decreases roughly to 10% at 30 arcsec from the guide star. This value of Strehl corresponds to a R-mag. of 16.6 for the pyramid and 15.5 for the Shack-Hartmann. Using these numbers and the described assumption we find for a median sky case (b=20, l=180) that the system sky coverage is 6,18,47 % for SHS and 11,33,82 % for PS in J,H and K band respectively.

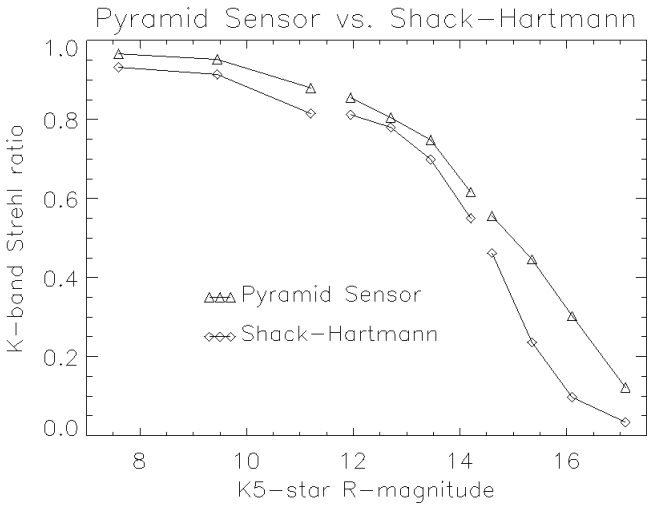

g 11. SR comparison between Pyramid and Shack-Hartmann obtaine as a function of the reference star magnitude

8. CONCLUSION

We have presented and discussed the design of the single conjugate AO system to be operational for the LBT single mirror first light scheduled for summer 2004. The AO system key elements are the Adaptive secondary mirror featuring 672 actuators and the Pyramid wavefront sensor having an adjustable pupil sampling with 10x10, 20x20 and 30x30 achievable using detector on chip binning. The WFS optical path is about 500mm long and the WFS unit is contained in a rectangular board of 400x320mm. The WFS is moveable to achieve a FOV of more than 2x2 arcminute. All the system components like, optical design, mechanical design, real time hardware, system expected performances has been analyzed with positive results. In particular simulations show a system limiting magnitude about 16.5 for 20% on-axis SR in K band leading to a median condition sky-coverage of 33%, a factor 2 better than a SHS system. AO system parts acquisition process has been started and we plan to begin the system integration in October 2002. First test of the AO system including the WFS and a 45 actuators prototype of the Adaptive Secondary are currently scheduled in the beginning of 2003.

9. REFERENCES

1. J.Hill, P.Salinari, "Large Binocular Telescope project ", *Astronomical Telescope and Instrumentation, SPIE Conf. 4837*, in press

2. J. Storm, W. Seifert, S. Bauer, F. Dionies, U. Hanschur, J. Hill, G. Moestl, P. Salinari, W Varava, H.Zinnecker, "Wavefront sensing and guiding units for the Large Binocular Telescope", *Proc. SPIE*, Vol. **4007**, p. 461-469, (2000) Adaptive Optical Systems Technology, Peter L. Wizinowich; Ed.

3. A.Riccardi, G.Brusa, P. Salinari, D. Gallieni, R. Biasi, M. Andrighettoni, H.M. Martin, "The adaptive secondary mirrors for the Large Binocular Telescope", *Astronomical Telescope and Instrumentation, SPIE Conf. 4839*, in press

4. H. Mandel, I. Appenzeller, D. Bomans, F. Eisenhauer et al.,"LUCIFER: a NIR spectrograph and imager for the LBT", *Proc. SPIE*, Vol. **4008**, p. 767-777, (2001), Optical and IR Telescope Instrumentation and Detectors, Masanori Iye; Alan F. Moorwood; Eds.

5. R. Ragazzoni, "Pupil plane wavefront sensing with an oscillating prism", *J Modern Optics*, **43**, 289 (1996)

6. R. Ragazzoni, J. Farinato, "Sensitivity of a pyramidic Wave Front sensor in closed loop Adaptive Optics", *Astronomy and Astrophysics*, v.**350**, p. L23-L26 (1999)

7. S. Esposito, A. Riccardi, "Pyramid Wavefront Sensor behavior in partial correction Adaptive Optic systems", *Astronomy and Astrophysics*, v.**369**, p. L9-L12 (2001)

8. D. Gallieni, E. Anaclerio, P.G. Lazzarini, A. Ripamonti, R. Spairani, C. Del Vecchio, P. Salinari, A. Riccardi, P. Stefanini, "LBT adaptive secondary units final design and construction", *Astronomical Telescope and Intrumentation, SPIE Conf. 4839*, in press

9. A.Riccardi, G.Brusa, P. Salinari, D. Gallieni, R. Biasi, M. Andrighettoni, H.M. Martin, "The adaptive secondary mirrors for the Large Binocular Telescope", *Astronomical Telescope and Instrumentation, SPIE Conf. 4839*, in press

10. E. Diolaiti, A. Tozzi, R. Ragazzoni, E. Viard, S. Esposito, A. Riccardi, J. Farinato, "Some novel concepts in multi pyramid wavefront sensing", *Astronomical Telescope and Intrumentation, SPIE Conf. 4839*, in press

11. R. Biasi, M. Andrighettoni, D. Veronese, V. Biliotti, L. Fini, A. Riccardi, "LBT adaptive secondary electronics ", *Astronomical Telescope and Intrumentation, SPIE Conf. 4839*, in press

12. M. Carbillet, L. Fini, B. Femenia, A. Riccardi, S. Esposito, E. Viard, F. Delplancke, N. Hubin, "CAOS simulation package 3.0 – an IDL based tool for adaptive optics systems design and simulations", *ASP Conf. Series*, v.**238**, p.249 (2001)

13. C. Vérinaud, M. Carbillet, B. Femenia, "CAOS (Code for Adaptive Optics Systems) Software package: New Developments ", *SF2A 2002, EDP-Sciences Conf. Series*, Ed. F. Combes, D. Barret, in press

14. J.N. Bahcall, R.M. Soneira, "Models for the galaxy and the predicted star counts" *Ap. J. Supp. Ser.*, **44**, pp. 73-110 (1980)

15. I.Foppiani, C.Baffa, V.Biliotti, G.Bregoli, G.Cosentino, E.Giani, S.Esposito, B.Marano, P.Salinari, "Photo counting CCDs as wavefront sensors for A.O.", *Astronomical Telescope and Instrumentation, SPIE Conf. 4837*, in press